JACS
JOURNAL OF THE AMERICAN CHEMICAL SOCIETY

Article

pubs.acs.org/JACS

Electrochemically Responsive Heterogeneous Catalysis for Controlling Reaction Kinetics

Xianwen Mao,[†] Wenda Tian,[†] Jie Wu,[‡] Gregory C. Rutledge,*[,†] and T. Alan Hatton*[,†]

[†]Department of Chemical Engineering and [‡]Department of Chemistry, Massachusetts Institute of Technology, 77 Massachusetts Avenue, Cambridge, Massachusetts 02139, United States

Supporting Information

ABSTRACT: We report a method to control reaction kinetics using electrochemically responsive heterogeneous catalysis (ERHC). An ERHC system should possess a hybrid structure composed of an electron-conducting porous framework coated with redox-switchable catalysts. In contrast to other types of responsive catalysis, ERHC combines *all* the following desired characteristics for a catalysis control strategy: continuous variation of reaction rates as a function of the magnitude of external stimulus, easy integration into fixed-bed flow reactors, and precise spatial and temporal control of the catalyst activity. Herein we first demonstrate a facile approach to fabricating a model ERHC system that consists of carbon microfibers with conformal redox polymer coating. Second, using a Michael reaction whose kinetics depends on the redox state of the redox polymer catalyst, we show that use of different electrochemical potentials permits continuous adjustment of the reaction rates. The dependence of the reaction rate on the electrochemical potential generally agrees with the Nernstian prediction, with minor discrepancies due to the multilayer nature of the polymer film. Additionally, we show that the ERHC system can be employed to manipulate the shape of the reactant concentration−time profile in a batch reactor through applying customized potential−time programs. Furthermore, we perform COMSOL simulation for an ERHC-integrated flow reactor, demonstrating highly flexible manipulation of reactant concentrations as a function of both location and time.

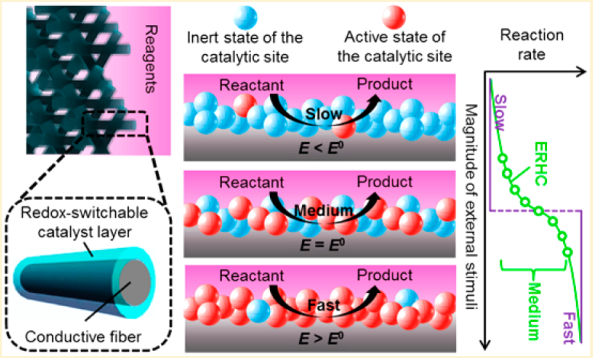

INTRODUCTION

The ability to exert control over an entity or a process is arguably the ultimate demonstration of our understanding of that process and enables the full exploitation of its potential. Stimuli-responsive systems offer advanced control methods because external signals can be exploited elegantly to regulate material properties.[1−5] Chemists have recently begun to incorporate control elements into catalyst design in response to an increasing interest in responsive catalytic systems. Such systems enable new strategies for the modulation of reaction kinetics using various chemico-physical stimuli.[6−10] The key to achieving stimuli-controlled catalysis is the development of a system in which the concentration or accessibility of the catalytic site in reaction media can be adjusted in response to external signals, such as temperature,[6−9] pH,[8] or solvent composition.[10] In most cases, the catalyst carrier (usually a soft material such as a polymeric gel) undergoes morphological and/or architectural changes upon exposure to an external stimulus that result in variations in the catalyst concentration and/or accessibility. For example, He et al.[6] used a thermoresponsive gel to move the catalyst into or out of the reaction medium, thus turning the reaction on or off at will. In another case, Wang et al.[8] used temperature or pH to de-swell a hydrogel, thereby concentrating the catalyst within the gel matrix and thus accelerating the reaction rate.

Herein we report a method to control reaction kinetics using electrochemically responsive heterogeneous catalysis (ERHC) (Figure 1). Our ERHC system possesses a hybrid structure consisting of two key components (Figure 1a): (i) an electron-conducting framework (e.g., interconnected conductive fibers) and (ii) conformal coating of this framework with redox-switchable catalysts whose activities can vary markedly with changes in redox states. One unique advantage of an ERHC system is that the electrochemical stimulus (i.e., potential) can be used to manipulate *continuously* the number of activated catalytic sites according to the Nernst equation.[11] Figure 1b illustrates a simple example case whereby the catalytic site is activated when oxidized, and deactivated when reduced. When the applied potential (E) on the conductive framework is much lower than the formal potential (E^0) of the redox-switchable catalyst, most catalytic sites are deactivated and thus the reaction is slow. When $E \gg E^0$, most catalytic sites are activated and thus the reaction is fast. In "on/off" bimodal catalysis (e.g., several responsive gel-based catalysts[6−10]), variations of external signals usually make reactions either fast or slow (Figure 1c, purple line). In contrast, in an ERHC system, the electrochemical potential can be employed to modulate the

Received: November 29, 2014
Published: January 6, 2015

DOI: 10.1021/ja512224g
J. Am. Chem. Soc. 2015, 137, 1348−1355

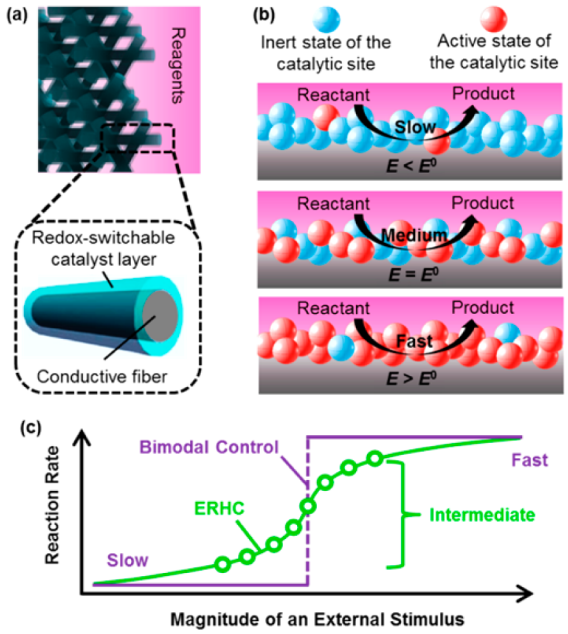

Figure 1. The ERHC concept. (a) Conceptual drawing of an ERHC system composed of interconnected conductive fibers with conformally coated with redox-switchable catalysts. (b) Schematic illustration of electrochemical control over the number of active sites and reaction rates. (c) Comparison between ERHC (green) and "on/off" bimodal responsive catalysis (purple) for kinetic control.

reaction rate continuously and thus achieve intermediate rates (Figure 1c, green data). Such flexible control over reaction rates is highly desirable in chemical synthesis, especially for mechanistic studies of reaction kinetics, selectivity control in complex reaction networks, and safe heat removal in exothermic reactions.[12−15]

More importantly, the electrochemical potential of an ERHC system can be varied locally in real-time with high resolution, allowing for precise spatial and temporal control of the catalyst's activity. Such exquisite control would benefit reaction engineering tremendously, a main objective of which is to adjust reactant distributions in reactors as functions of both location and time.[13,16−19] For controlled catalysis, chemical (e.g., pH or solvent type) and thermal stimuli are commonly adopted. However, although there are several ways to introduce chemical species (e.g., dripping) and thermal energy (e.g., conventional or microwave heating) into a system, precise control of chemical activity over location and time is difficult to achieve (especially in a flow system) and is further hampered by mass diffusion or heat dissipation processes.

Additionally, an ERHC system allows easy integration into fixed-bed flow reactors, because, unlike soft materials-based catalysts, activation/deactivation of the ERHC system does not lead to significant changes in volume. Therefore, ERHC meets a major goal of modern chemistry, that is, to combine the advantages of heterogeneous catalysis and flow chemistry to enhance the sustainability of chemical synthesis practices.[12,20,21] However, many of the soft materials-based catalysts[6−10] undergo significant morphological/structural changes (e.g., volumetric[6,8−10] and sol−gel[7] transitions) during the activation/deactivation process, and hence these systems cannot be used easily in a fixed bed reactor that requires a fixed catalyst volume and no catalyst leaching.[21,22]

The ERHC concept is broadly applicable to a variety of important reactions that can be catalyzed by redox-switchable catalysts.[23−28] This electrochemical modulation method may also be employed to tune redox properties of the active sites in enzymes, offering novel control strategies in enzyme catalysis.[29,30] Moreover, porous electrodes with tunable pore size and surface area (e.g., electrospun carbon fiber webs)[31,32] may be used as the conductive framework in an ERHC system, providing possibilities to facilitate reactant diffusion and improve catalysis performance.

RESULTS AND DISCUSSION

Fabrication and Characterization of a Model ERHC System. The proof-of-concept ERHC system developed here consists of a porous carbon fiber (CF) matrix with conformally coated polyvinylferrocene (PVF). Ferrocene can function either directly as a catalyst with a redox-controlled activity,[28] or indirectly as a redox-active ligand to adjust the reactivity of metal complexes.[26] The CF matrix serves as the electron-conducting framework in this ERHC system. The PVF/CF hybrid system was prepared by electrochemical oxidation-induced deposition of PVF to the CF matrix (Figure 2a).[33] For details, see the Experimental Section. Application of a positive electrochemical potential (0.8 V) to the CF matrix provides a localized oxidative environment on the fiber surface. The affinity of ferrocene for hydrophobic organic solvents (e.g., chloroform) is reduced upon oxidation.[33,34] Therefore, PVF

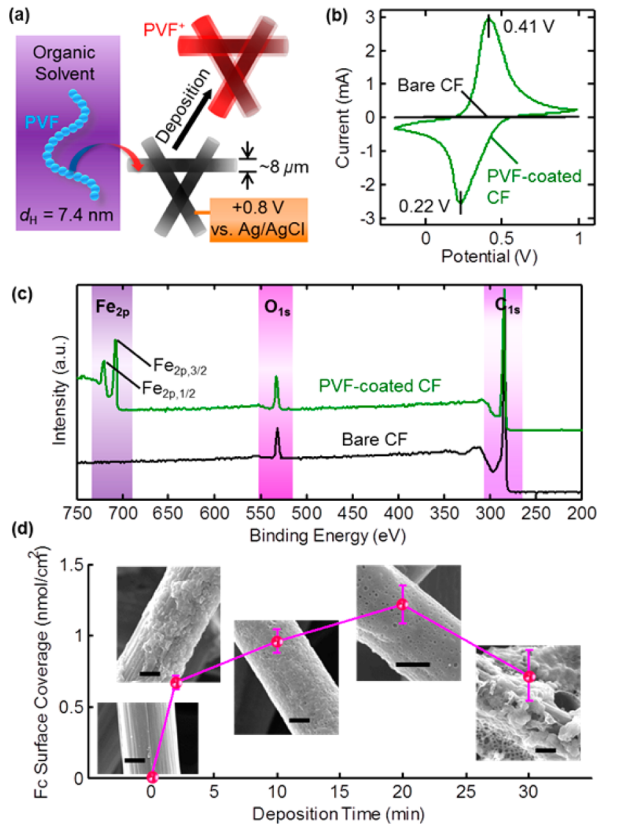

Figure 2. Preparation of PVF/CF hybrids. (a) Schematics of oxidation-induced conformal deposition of PVF onto CFs. (b) CVs of a bare and a PVF-coated CF matrix. Scan rate: 50 mV/s. Electrolyte: 0.5 M $NaClO_4$. (c) XPS spectra of a bare and a PVF-coated CF matrix. (d) Ferrocene surface coverage versus deposition time. Insets: corresponding SEM images of the specimens. Scale bar: 2 μm.

DOI: 10.1021/ja512224g
J. Am. Chem. Soc. 2015, 137, 1348−1355

initially soluble in chloroform becomes solvophobic and subsequently precipitates onto the fiber when it is oxidized at the fiber surface. The hydrodynamic diameter (d_H) of the polymer (molecular weight = 50 000 g/mol) in chloroform was ~7.4 nm.[33] The diameter of the carbon fiber was around 8 μm.

The presence of ferrocene moieties in an as-prepared hybrid system was verified by cyclic voltammetry (CV) (Figure 2b). The PVF-coated CF matrix prepared by a 10 min potentiostatic deposition at 0.8 V showed pronounced anodic and cathodic peaks at 0.41 and 0.22 V, respectively, characteristic of ferrocene.[35] The unmodified CF substrate showed no such signals. Figure 2c shows the wide-range X-ray photoelectron spectra (XPS) of the unmodified CFs and the PVF-coated CFs. The spectrum of PVF-coated CFs possesses a C_{1S} peak at 281 eV, an O_{1S} peak at 532 eV, and two Fe_{2p} peaks at 708 eV (2p 3/2) and 721 eV (2p 1/2) due to the spin−orbital splitting of the iron p orbital. The spectrum of the unmodified CFs does not exhibit such Fe_{2p} peaks. The XPS results, complementary to the CV analysis, confirm the successful surface functionalization of CFs by PVF.

The key factor to controlling the quality of the PVF coating is the potentiostatic deposition time. Scanning electron microscopy (SEM) images (Figure 2d insets) show a clear morphological transition in the CF surfaces with different deposition times. An unmodified CF exhibits a clean surface. Deposition for 2 min led to non-uniform PVF aggregates that only partially covered the fiber surface. With 10 and 20 min deposition times, conformal, uniform coating around fibers with complete surface coverage was achieved. However, a further increase in deposition time to 30 min led to uneven coating and cracking of the PVF film; we also observed that the initially deposited film fell off the CF matrix in this latter case. This poor coating quality might be due to the large thickness of the polymer film and the low solubility of PVF^+; both factors could lead to mechanical instability of the deposited film.

To evaluate quantitatively the deposition efficacy, we used CV measurements to estimate the ferrocene surface coverage (Γ_{Fc}, nmol/cm^2) on the CFs (Figure 2d). For calculation details, see the Experimental Section. Γ_{Fc} increased with deposition time in the range of 0−20 min, but decreased over the period from 20 to 30 min. This later decay indicates loss of PVF, consistent with the SEM observation. Thus, an intermediate deposition time (10−20 min) was thought to be optimal since it consistently generated uniform conformal PVF coatings. Large-area SEM images of unmodified CFs, and PVF-coated CFs with 10 and 30 min deposition time are shown in Figure 3.

Energy dispersive X-ray spectroscopic (EDS) elemental mapping of Fe corroborated the assertion that the PVF-coated CF substrate (10 min deposition) was completely covered by the polymer (Figure 4a). In contrast, the EDS image of a bare CF substrate exhibits negligible Fe signals (Figure 4b). Additionally, the cross-sectional EDS (Fe and C) images of a cryo-fractured sample indicates a clear core (C)−shell (Fe) hybrid structure (Figure 4c).

Continuous Adjustment of Reaction Rates Using ERHC. The model reaction chosen for demonstrating the use of ERHC to control kinetics is the Michael addition of methyl vinyl ketone (MVK) and ethyl-2-oxycyclopentane carboxylate (E2OC) (Figure 5a). This class of reactions is important for steroid synthesis and for forming carbon−carbon bonds in many other organic compounds.[36] Ferrocenium (Fc^+) catalyzes this reaction as a Lewis acid whereas ferrocene (Fc) has no

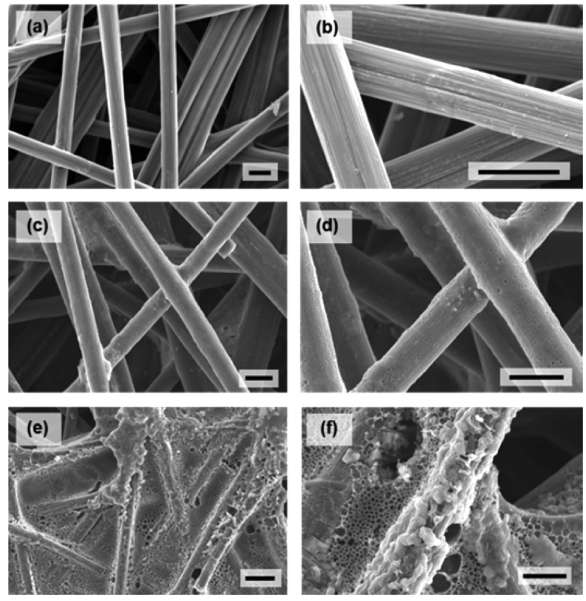

Figure 3. Large-area SEM images of (a,b) unmodified CFs, (c,d) PVF-coated CFs with 10 min deposition, and (e,f) PVF-coated CFs with 30 min deposition. Scale bar: 10 μm.

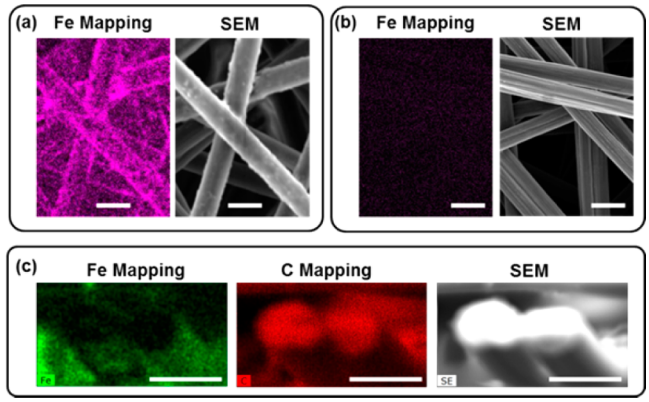

Figure 4. EDS elemental mapping. (a) Fe mapping and corresponding SEM image of PVF-coated CFs (10 min deposition). (b) Fe mapping and corresponding SEM image of unmodified CFs. (c) Fe mapping, C mapping, and corresponding SEM image of the cross section of cryo-fractured PVF-coated CFs (10 min deposition). Scale bar: 10 μm.

catalytic activity toward this reaction.[28] This reaction is pseudo-first order in MVK; such kinetic characteristics indicate that E2OC reacts reversibly with the catalyst to form an adduct which then reacts more slowly with MVK.[28] The ERHC concept may be broadly applicable to other types of Lewis acid-catalyzed reactions of scientific and technological significance, such as alkene alkylation, Friedel−Crafts reactions, aldol reactions, and heterocyclic ring aperture.[37] For heterogeneous catalysis, it is convenient and conventional to express the reaction rate as moles of reactants reacted per unit mass of the catalyst.[22] Thus, the rate law is written as $-r$ (mol/(g catalyst·min)) = $-dm/dt = k_{app}m$, where m is the concentration of MVK normalized to the catalyst mass (mol/g catalyst), and k_{app} is the apparent first-order rate constant (min^{-1}). Integration of this differential equation results in $\ln m = -k_{app}t + \ln m_0$, where m_0 is the initial concentration of MVK. Figure 5b shows $\ln m$ versus the reaction time, measured in the presence of a PVF/CF system prepared by 10 min potentiostatic deposition. For

DOI: 10.1021/ja512224g
J. Am. Chem. Soc. 2015, 137, 1348−1355

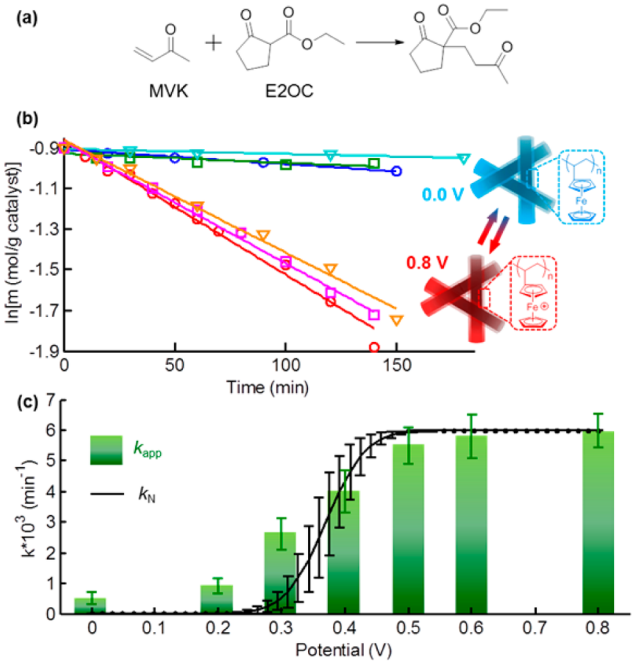

Figure 5. (a) Schematics of the Michael addition reaction of methyl vinyl ketone and ethyl 2-oxycyclopentanecarboxylate. (b) ln m versus t when 0.8 and 0.0 V were applied. Different symbols indicate three independent measurements. (c) k_{app} (green) and k_N (black) as a function of potential. Error bars for k_{app} were obtained from four or five measurements using different electrodes prepared under identical conditions. Error bars for k_N were from the standard deviation of the E^0 value for ferrocene.

details on the kinetic measurement, see the Experimental Section. When a potential of 0.8 V (which provides 100% conversion of Fc to Fc^{+}[35]) was applied, m decayed markedly with time. Linearity between ln m and t confirms the pseudo-first order kinetics. When the potential was set at 0.0 V, m remained almost unchanged. Three independent measurements led to a $k_{app}^{0.8\ V} = (6.0 \pm 0.5) \times 10^{-3}$ min^{-1} and a $k_{app}^{0.0\ V} = (0.5 \pm 0.2) \times 10^{-3}$ min^{-1}, indicating that the PVF/CF catalyst showed strong catalytic activity at 0.8 V and almost no activity at 0.0 V. A potential of 0.8 V applied to a bare CF matrix did not cause a concentration decay of MVK (Supporting Information (SI) Figure S2). Chronoamperometry measurements (SI Figure S3) show that the time scale for catalyst activation (i.e., converting Fc to Fc$^+$ electrochemically) was ~5 s. Scaling analysis (SI Section S1) suggests that under our experimental conditions the reactant mass transport time scale was ~0.1 s. Both these time scales were significantly shorter than the reaction time scale ($1/k_{app}^{0.8\ V}$ is ~167 min); hence the activation and transport processes had negligible influence on the determination of k_{app}.

To demonstrate the unique ability of an ERHC system to control kinetics on demand and achieve multiple intermediate reaction rates, we applied a series of different potentials between 0.8 and 0.0 V to the PVF/CF system and measured the corresponding reaction rates. As shown in Figure 5c (green bar), we obtained intermediate k_{app} values that were higher than $k_{app}^{0.0\ V}$ and lower than $k_{app}^{0.8\ V}$. Figure 5c (black data) also shows the rate constants predicted theoretically based upon the Nernst equation: $k_N = k^{OX}\beta/(1 + \beta)$, with $\beta = \exp(F(E - E^0)/RT)$, where k^{OX} is the rate constant when the catalyst is completely oxidized (i.e., $k_{app}^{0.8\ V}$), F is the Faraday constant, E^0 is the standard redox potential for ferrocene, determined to be 0.370 ± 0.025 V from five CV measurements, R is the ideal gas constant, and T is the reaction temperature (298 K). Figure 5c shows that k_{app} was generally consistent with k_N, but exhibited a less steep trend with decreasing potential than did k_N. Specifically, when the potential was at low values (0.0, 0.2, and 0.3 V), k_{app} was larger than k_N. One possible explanation for the difference between k_{app} and k_N is that the PVF coating may have been a multilayer film whose redox composition did not exhibit an ideal Nernstian dependence on potential; only a redox monolayer can exhibit ideal Nernstian behavior.[38] In a multilayer film, each layer of ferrocene may experience a slightly different potential. Thus, ferrocene molecules at the outermost layer may still have been in the oxidized state even when the electrode surface was at potentials much lower than E^0; note that the as-prepared PVF/CF system contained only Fc$^+$. The multilayer nature of the PVF coating was further elucidated by using a redox polymer electrode (RPE) model to simulate the instantaneous amperometric response of PVF during linear potential sweeping (see SI Section S2).

Temporal Control in Batch Systems. To demonstrate the ability of ERHC to exert temporal control over reaction kinetics, we followed the concentration of MVK in a batch reactor while using the electrochemical potential to modulate the catalytic activity of the PVF/CF hybrid at different times. Figure 6 shows the concentration of MVK in mol/L (C_{MVK}) in

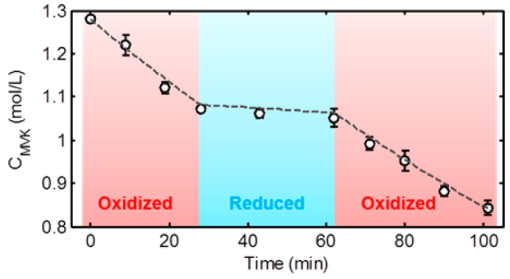

Figure 6. Concentration of MVK (purple circle) in a batch reactor as a function of time in the presence of a PVF/CF hybrid (10 min deposition), whose electrochemical potential was programmed to be 0.8 V (completely oxidized state) from 0 to 28 min, and 0.0 V (completely reduced state) from 28 to 64 min, and 0.8 V (completely oxidized state) again from 64 to 100 min. Error bars were obtained from three measurements using different electrodes prepared under identical conditions. The gray dash line shows the prediction from the batch system mass balance equations using the $k_{app}^{0.8\ V}$ and $k_{app}^{0.0\ V}$ values.

the reaction medium as a function of time, with the electrochemical potential of the PVF/CF catalyst set to be at 0.8 V from 0 to 28 min (fully oxidized state), 0.0 V from 28 to 64 min (fully reduced state), and 0.8 V from 64 to 100 min. Switching in situ between 0.8 and 0.0 V effectively turned the reaction on and off, respectively. In Figure 6, C_{MVK} decayed in the first 28 min, remained almost unchanged for the next 36 min, and continued to decay afterward. Such a concentration–time profile was consistent with the prediction (gray dash lines) based upon the batch reactor mass balance equations using the $k_{app}^{0.0\ V}$ and $k_{app}^{0.8\ V}$ values. This consistency also suggested that the activation/deactivation of the catalyst was rapid, causing no apparent discrepancy between the experimentally measured profile and the prediction (which assumed that the activation or deactivation process happened instantaneously). This rapid

DOI: 10.1021/ja512224g
J. Am. Chem. Soc. 2015, 137, 1348–1355

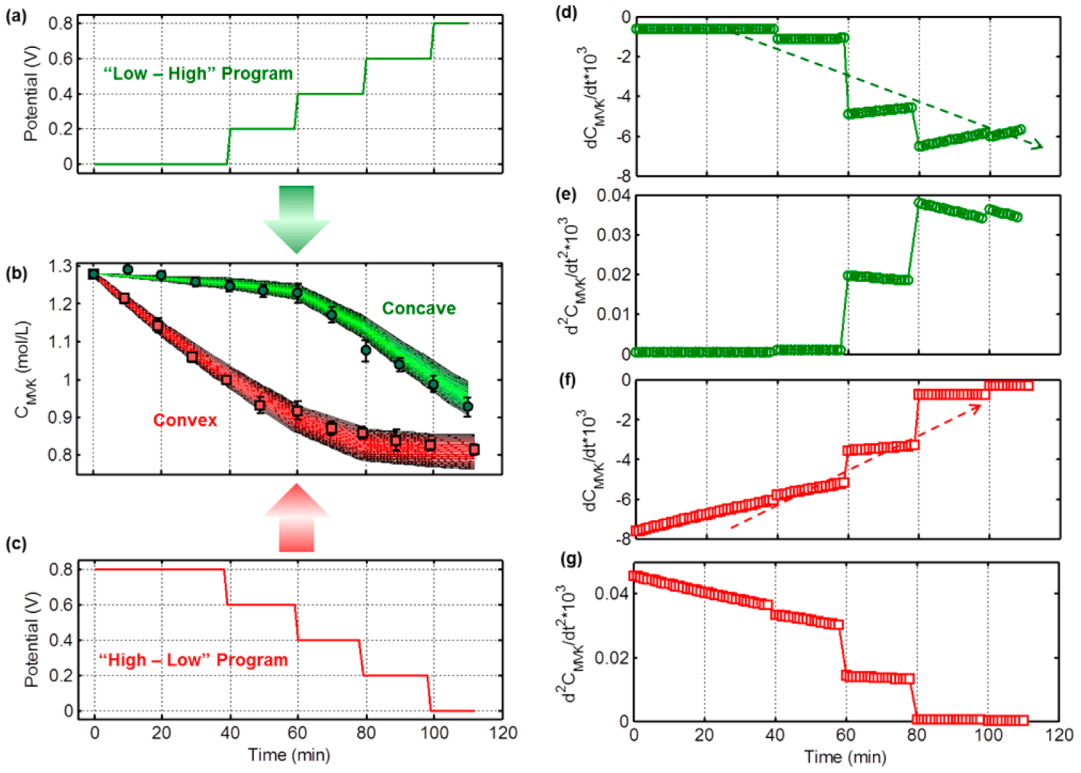

Figure 7. (a–c) The C_{MVK}–t relationships (b) in a batch reactor when two different potential–time profiles (a,c) were applied. The green circles or red squares are experimentally determined concentrations. Error bars were obtained from three measurements using different electrodes prepared under identical conditions. The shaded bands are the predictions from the batch system mass balance relationship using the $k_{app}^{0.8\ V}$, $k_{app}^{0.6\ V}$, $k_{app}^{0.4\ V}$, $k_{app}^{0.2\ V}$, and $k_{app}^{0.0\ V}$ values. (d,e) The first derivative (dC_{MVK}/dt) (d) and second derivative (d^2C_{MVK}/dt^2) (e) of the green line (theoretical) shown in (b). (f,g) The first derivative (dC_{MVK}/dt) (f) and second derivative (d^2C_{MVK}/dt^2) (g) of the red line (theoretical) in (b).

catalyst activation/deactivation should be attributed to the fast electron transfer kinetics of the ferrocene moiety.[38]

More interestingly, ERHC could be employed to create a complicated shape of the reactant concentration–time profile through applying a customized potential–time program. Figure 7 shows such an example. By applying two different potential–time profiles, termed "low–high" (Figure 7a) and "high–low" (Figure 7c) programs, we obtained two very different C_{MVK}–t curves (Figure 7b). The "low–high" program resulted in a slow decay in C_{MVK} in the first 60 min followed by a fast decay from 60 to 112 min, whereas the "high–low" program led to a fast concentration decrease from 0 to 80 min and a slower decrease from 80 to 112 min. The two shaded bands with asymptotic color changes in Figure 7b were predictions from the batch system mass balance equations with first-order kinetics using the $k_{app}^{0.8\ V}$, $k_{app}^{0.6\ V}$, $k_{app}^{0.4\ V}$, $k_{app}^{0.2\ V}$, and $k_{app}^{0.0\ V}$ values and their standard deviations. The experimental data (circles and squares in Figure 7b) were in good agreement with the predictions.

It is also interesting to note that, when employing the "low–high" program, the overall shape of the C_{MVK}–t curve exhibited a somewhat concave character, even though, in each segment with a constant potential value, the C_{MVK}–t relationship was convex in nature. This convex character is clearly seen on examination of the first and second derivatives of the calculated C_{MVK}–t curve: in each individual segment, the first derivative (dC_{MVK}/dt) was an increasing function of time (Figure 7d), and the second derivative (d^2C_{MVK}/dt^2) was positive (Figure 7e). In fact, it would be possible to obtain a "real" concave curve by using very small increments in potential, for example, using a linear potential–time function. On the other hand, with the "high–low" program, the C_{MVK}–t relationship exhibited a convex shape, with different decay constants ($\tau^P = 1/k_{app}^P$, P is the applied potential with values of 0.0, 0.2, 0.4, 0.6, and 0.8 V) in each constant-potential segment. The first and second derivatives in this case are shown in Figure 7f and 7g, respectively. The distinction between the "low–high" case and the "high–low" case can be also appreciated by comparing Figure 7d with Figure 7f. In both cases, dC_{MVK}/dt in each *individual* segment was an increasing function of t. With the "high–low" program, dC_{MVK}/dt exhibited a general increasing trend with time (indicated by the dashed arrow in Figure 7f). However, with the "low–high" program, dC_{MVK}/dt exhibited a general decreasing trend with time (indicated by the dashed arrow in Figure 7d). This general decreasing trend gave rise to the apparently concave shape of the C_{MVK}–t curve in Figure 7b.

Temporal and Spatial Control in Flow Systems Demonstrated by COMSOL Simulation. A distinct advantage of integrating ERHC into a flow reactor is the flexible control over reactant concentrations as a function of both location and time. We note that the spatial control in a flow reactor may be unique to an ERHC system, due to its heterogeneous nature combined with the fact that the electrochemical stimulus can be applied *locally* with high precision. To demonstrate the capability of ERHC to exert both spatial and temporal control in a flow reactor, we performed a COMSOL simulation on an ERHC-integrated packed-bed-like tube reactor, composed of ~40 000 stacked PVF/CF sheets whose activity can be adjusted individually in real-time by changes in their electrochemical potentials. The tube reactor

DOI: 10.1021/ja512224g
J. Am. Chem. Soc. 2015, 137, 1348–1355

model is illustrated schematically in Figure 8a. The reactor was taken to be 10 m long and 1 m in diameter, with a catalyst mass

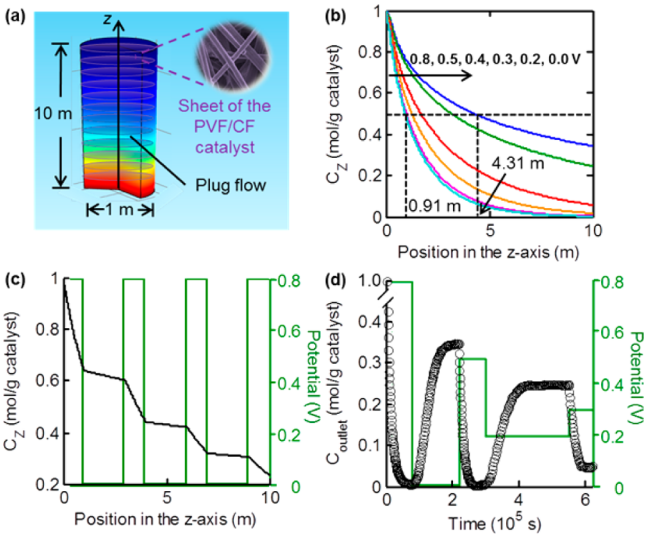

Figure 8. (a) Schematics of the ERHC-integrated flow reactor employed in the COMSOL simulation. (b) C_Z as a function of the axial position within the reactor when a series of different potentials were applied to all the catalyst sheets. (c) The applied potential (green) and the corresponding C_Z (black) as a function of position in the z-direction. (d) The applied potential (green) and the corresponding concentration C_{outlet} (black) as a function of time.

of 1700 kg and a packing density of 217 kg/m^3. The inlet concentration of MVK was fixed at 1 mol/g catalyst. For simulation details, see SI Section S3. Figure 8b shows the concentration of MVK (C_Z) versus position along the z-axis of the reactor when a constant potential was applied to all the catalyst sheets, for different such potentials. Clearly, with increasing potential, C_Z decreased more quickly. For instance, when 0.0 V was applied, C_Z decayed by half at z = 4.31 m, whereas with an applied potential of 0.8 V, C_Z decreased by half at z = 0.91 m. Conceivably, more complicated concentration profiles can be obtained by applying different potentials at different positions within the reactor. Figure 8c shows such an example: a step-like concentration profile (black line) was obtained through application of a square-wave-like potential profile (green line). To further demonstrate temporal control, we arbitrarily changed the potentials of all the catalyst sheets over time (Figure 8d, green line). Consequently, an interesting relationship between the outlet concentration of MVK (C_{outlet}) *and* time was predicted (Figure 8d, black line). In this case, an initial condition with a uniform MVK concentration of 1 mol/g catalyst throughout the reactor was applied. The results shown in Figure 8c,d suggest that ERHC allows flexible spatial and temporal manipulation of reactant concentrations; such a high degree of flexibility is almost unattainable using conventional control strategies.

Tests of Other Reactions. We measured k_{app} values for six other Michael addition reactions using the PVF/CF catalysts (10 min deposition); the results are summarized in Figure 9. Reactions (a), (b), (c), and (d) were found to show much higher k_{app} values under the completely oxidized state (i.e., 0.8 V) than at the completely reduced conditions (i.e., 0.0 V). We also tested one intermediate potential (0.3 V), which gave rise to a rate between the $k_{app}^{0.0\ V}$ and $k_{app}^{0.8\ V}$ values for these four reactions. Results shown in Figure 9a–d indicate that the ERHC control strategy could also be applied to these four reactions using the PVF/CF hybrid. However, the k_{app} values for reactions (e) and (f) were very low, and showed no significant difference across different potentials. It was found previously that, for iron(III) catalysis of the Michael reaction of β-dicarbonyl compounds and enones, fast kinetics were observed for reactions involving either cyclic ketoesters or methyl vinyl ketone or both.[39] Reactions (e) and (f) involve neither ketoesters nor methyl vinyl ketone.

CONCLUSION

In this study, we have demonstrated a control strategy to manipulate reaction kinetics through electrochemically responsive heterogeneous catalysis (ERHC). We demonstrated a facile electrochemical method with high controllability to fabricate a proof-of-concept ERHC system that consisted of interconnected carbon fibers with conformal PVF coating. The surface functionalization efficiency could be varied systematically by potentiostatic deposition time. This fabrication approach is very versatile; other functional components, such as aniline, pyrrole, carbon nanotubes and graphene oxides, could be electrochemically co-deposited with PVF to improve the catalysis performance.

Second, using a model first-order reaction whose kinetics depends on the redox state of the PVF catalyst, we showed that different electrochemical potentials could be used to vary the reaction rates *continuously*. The dependence of the reaction rate on the electrochemical potential was generally consistent with the Nernstian prediction.

Additionally, we showed that, in a batch system, the PVF/CF ERHC system could be utilized to manipulate the shape of the reactant concentration–time profile through applying customized potential–time programs. We also carried out COMSOL simulation for an ERHC-integrated flow reactor, demonstrating highly flexible control over reactant concentrations as a function of both location and time. Such a high degree of flexibility in spatial and temporal control is almost unattainable using conventional control strategies.

In contrast to other types of stimuli-triggered catalysis,[6−10] ERHC combines all the following advantageous features: continuous variation of reaction rates, easy integration into fixed-bed flow reactors, and precise spatial and temporal control over the catalyst activity. This electrochemical modulation method is broadly applicable to a variety of reactions amenable to redox-switchable catalysis,[23−28] and may potentially offer new control strategies in enzyme catalysis.[29,30] The conductive framework in an ERHC system may accommodate porous carbon electrodes with tunable morphologies and electronic properties,[40] allowing further optimization of transport properties, electron transfer kinetics, and catalysis performance. With broad applicability and high design flexibility, ERHC could pave the way to intriguing novel applications in controlled catalysis, chemical synthesis and reaction engineering.

EXPERIMENTAL SECTION

Chemicals and Materials. Polyvinylferrocene (molecular weight = 50 000 g/mol) was obtained from Polysciences. Methyl vinyl ketone, ethyl 2-oxycyclopentanecarboxylate, 2-acetylcyclopentanone, ethyl acetoacetate, ethyl 2-ethylacetoacetate, *trans*-4-phenyl-3-buten-2-one, sodium perchlorate, tetrabutylammonium perchlorate, and chloroform were purchased form Sigma-Aldrich. Deuterated methanol was purchased from Cambridge Isotope Laboratories. All reagents were

DOI: 10.1021/ja512224g
J. Am. Chem. Soc. 2015, 137, 1348–1355

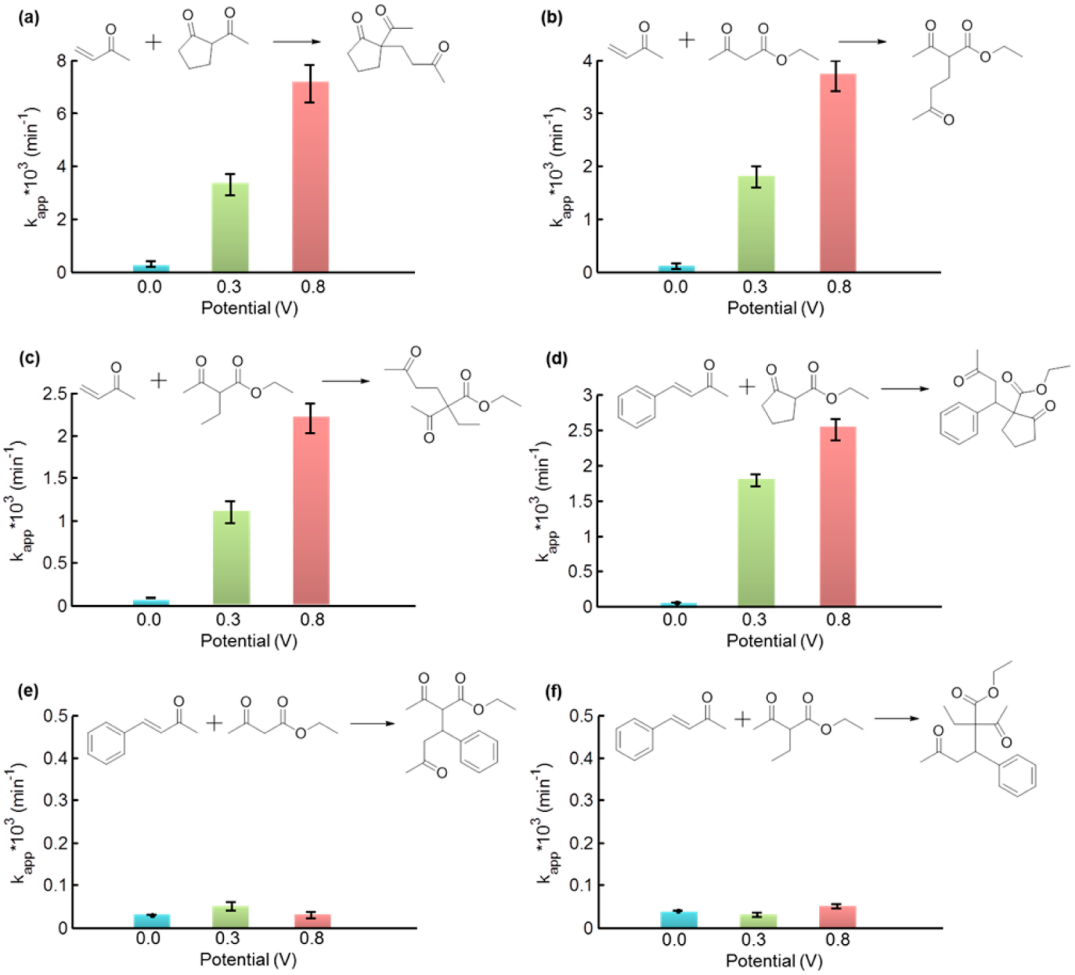

Figure 9. k_{app} values obtained at three different electrochemical potentials using the PVF/CF hybrids as the catalysts for six other Michael addition reactions: (a) methyl vinyl ketone + 2-acetylcyclopentanone; (b) methyl vinyl ketone + ethyl acetoacetate; (c) methyl vinyl ketone + ethyl 2-ethylacetoacetate; (d) *trans*-4-phenyl-3-buten-2-one + ethyl 2-oxycyclopentanecarboxylate; (e) *trans*-4-phenyl-3-buten-2-one + ethyl acetoacetate; (f) *trans*-4-phenyl-3-buten-2-one + ethyl 2-ethylacetoacetate. Error bars were obtained from three to four measurements using different electrodes prepared under identical conditions.

used as received throughout the study, without further purification or chemical modification unless otherwise noted. A platinum wire auxiliary electrode and an Ag/AgCl (3 M NaCl) reference electrode were purchased from BASi.

Instrumentation. Scanning electron microscopy (JEOL-6010LA) was used to investigate the morphologies of the PVF/CF catalysts and perform energy dispersive elemental mapping. X-ray photoelectron spectra were recorded with a Kratos Axis Ultra instrument equipped with a monochromatic Al Kα source operated at 150 W. Electrochemical experiments were performed on an AutoLab PGSTAT 30 potentiost at with GPES software. All potentials in this work are referred to a Ag/AgCl (3 M NaCl) reference electrode. ^{1}H NMR analysis was performed in deuterated methanol with a Bruker 400. The nitrogen adsorption/desorption measurements were performed with ASAP2020, Micromeritics.

Fabrication of PVF/CF Hybrids. A carbon fiber matrix (Toray, TGP-H-060) with a nominal surface area of 1 cm^2 and a thickness of 200 μm was immersed in 5 mL of chloroform solution containing 0.1 M tetrabutylammonium perchlorate and 10 mg/mL PVF. An electrochemical potential of 0.8 V versus Ag/AgCl was applied to the carbon fiber matrix for a period of 2, 10, 20, and 30 min to induce the PVF deposition process. The surface functionalization efficiency (i.e., ferrocene surface coverage) was calculated from the cyclic voltammograms according to the following equation:[41]

$$\Gamma = \int_{V_1}^{V_2} [i_a(V) - i_c(V)]\, dV/(2Av_s eN_A) \quad (1)$$

where Γ is the ferrocene surface coverage, V_1 and V_2 are the cutoff potentials in cyclic voltammetry, $i_a(V)$ and $i_c(V)$ are the instantaneous anodic and cathodic currents as a function of potential, v_s is the scan rate, e is the elementary charge, N_A is Avogadro's number, and A is the total surface area of the CF matrix (calculated by the mass of the CF matrix multiplied by its specific surface area, determined by nitrogen adsorption isotherms by means of the Brunauer–Emmett–Teller method). Note that eq 1 does not consider the charging current because it was negligible compared to the faradiac current of ferrocene under our experimental conditions. Equation 1 is a universal expression to calculate total charges; it applies to cyclic voltammograms of any shape since it uses the integral area of the cyclic voltammogram/scan rate to represent the sum of anodic and cathodic voltammetric charges.[41]

Kinetic Measurements. Equimolar mixtures of reactants (1 mL of E2OC and 0.58 mL of MVK) and the supporting electrolyte (68 mg of sodium perchlorate) were added to 4 mL of methanol. The reaction between E2OC and MVK was carried out in an electrochemical cell with the PVF/CF catalyst as the working electrode, a platinum wire as the counter electrode, and an Ag/AgCl electrode as the reference electrode. The reaction mixture was magnetically stirred at a speed of 220 rpm and kept at 298 K using a water bath. The progress of the reaction was followed by the time dependence of the vinyl proton

DOI: 10.1021/ja512224g
J. Am. Chem. Soc. 2015, 137, 1348–1355

NMR signal at 6.3 ppm.[28] Aliquots of 0.1 mL were taken from the 4 mL reaction mixture and mixed with 0.7 mL of deuterated methanol for NMR analysis. The typical sampling frequency was around 10−20 min. Similar procedures were adopted for other reactions shown in Figure 9.

COMSOL Simulation. Simulations were carried out with the COMSOL (Multiphysics Version 4.2a) software package. The plug flow module was used under either transient or steady state conditions with first-order reaction kinetics for MVK. The relationship between the potential applied and the corresponding reaction rate constant was determined experimentally (see Figure 5c). The total mass of the catalyst (1700 kg), or the size of the reactor (10 m in length and 1 m in diameter), was chosen such that when the catalyst was fully oxidized (fixed at a potential of 0.8 V), the concentration of MVK decayed to zero at the outlet. The mass of the catalyst and the volume of the reactor were correlated from the density of the PVF/CF catalyst. There were approximately 40 000 sheets in the tube reactor. Details for the COMSOL simulation are shown in SI Section S3.

■ ASSOCIATED CONTENT

Supporting Information

Scaling analysis of the reactant transport process, details of the RPE simulation, details of the COMSOL simulation, and supplementary figures. This material is available free of charge via the Internet at http://pubs.acs.org.

■ AUTHOR INFORMATION

Corresponding Authors

*rutledge@mit.edu

*tahatton@mit.edu

Notes

The authors declare no competing financial interest.

■ ACKNOWLEDGMENTS

We acknowledge the MITEI Seed Fund Grant for financial support.

■ REFERENCES

(1) Stuart, M. A. C.; Huck, W. T. S.; Genzer, J.; Muller, M.; Ober, C.; Stamm, M.; Sukhorukov, G. B.; Szleifer, I.; Tsukruk, V. V.; Urban, M.; Winnik, F.; Zauscher, S.; Luzinov, I.; Minko, S. *Nat. Mater.* **2010**, *9*, 101−113.

(2) Mura, S.; Nicolas, J.; Couvreur, P. *Nat. Mater.* **2013**, *12*, 991−1003.

(3) Fleischmann, E. K.; Zentel, R. *Angew. Chem., Int. Ed.* **2013**, *52*, 8810−8827.

(4) Doring, A.; Birnbaum, W.; Kuckling, D. *Chem. Soc. Rev.* **2013**, *42*, 7391−7420.

(5) Wiese, S.; Spiess, A. C.; Richtering, W. *Angew. Chem., Int. Ed.* **2013**, *52*, 576−579.

(6) He, X. M.; Aizenberg, M.; Kuksenok, O.; Zarzar, L. D.; Shastri, A.; Balazs, A. C.; Aizenberg, J. *Nature* **2012**, *487*, 214−218.

(7) Rodríguez-Llansola, F.; Escuder, B.; Miravet, J. F. *J. Am. Chem. Soc.* **2009**, *131*, 11478−11484.

(8) Wang, Y.; Zhang, J. Z.; Zhang, W. Q.; Zhang, M. C. *J. Org. Chem.* **2009**, *74*, 1923−1931.

(9) Lu, Y.; Yuan, J. Y.; Polzer, F.; Drechsler, M.; Preussners, J. *ACS Nano* **2010**, *4*, 7078−7086.

(10) Wang, G. Q.; Kuroda, K.; Enoki, T.; Grosberg, A.; Masamune, S.; Oya, T.; Takeoka, Y.; Tanaka, T. *Proc. Natl. Acad. Sci. U.S.A.* **2000**, *97*, 9861−9864.

(11) Bard, A. J.; Faulkner, L. R.: *Electrochemical methods: fundamentals and applications*, 2nd ed.; Wiley: New York, 2001.

(12) Newman, S. G.; Jensen, K. F. *Green Chem.* **2013**, *15*, 1456−1472.

(13) Yoshida, J. I.; Kim, H.; Nagaki, A. *ChemSusChem* **2011**, *4*, 331−340.

(14) Vilekar, S. A.; Fishtik, I.; Datta, R. *Chem. Eng. Sci.* **2010**, *65*, 2921−2933.

(15) Renken, A.; Kiwi-Minsker, L. *Adv. Catal.* **2010**, *53*, 47−122.

(16) Reyes, D. R.; Iossifidis, D.; Auroux, P. A.; Manz, A. *Anal. Chem.* **2002**, *74*, 2623−2636.

(17) Auroux, P. A.; Iossifidis, D.; Reyes, D. R.; Manz, A. *Anal. Chem.* **2002**, *74*, 2637−2652.

(18) Wiles, C.; Watts, P. *Green Chem.* **2012**, *14*, 38−54.

(19) Stoll, R. S.; Hecht, S. *Angew. Chem., Int. Ed.* **2010**, *49*, 5054−5075.

(20) Astruc, D.; Lu, F.; Aranzaes, J. R. *Angew. Chem., Int. Ed.* **2005**, *44*, 7852−7872.

(21) Gross, E.; Liu, J. H. C.; Toste, F. D.; Somorjai, G. A. *Nat. Chem.* **2012**, *4*, 947−952.

(22) Fogler, H. S. *Elements of Chemical Reaction Engineering*, 4th ed.; Prentice Hall PTR: Upper Saddle River, NJ, 2006.

(23) Broderick, E. M.; Guo, N.; Vogel, C. S.; Xu, C. L.; Sutter, J.; Miller, J. T.; Meyer, K.; Mehrkhodavandi, P.; Diaconescu, P. L. *J. Am. Chem. Soc.* **2011**, *133*, 9278−9281.

(24) Broderick, E. M.; Guo, N.; Wu, T. P.; Vogel, C. S.; Xu, C. L.; Sutter, J.; Miller, J. T.; Meyer, K.; Cantat, T.; Diaconescu, P. L. *Chem. Commun.* **2011**, *47*, 9897−9899.

(25) Gregson, C. K. A.; Gibson, V. C.; Long, N. J.; Marshall, E. L.; Oxford, P. J.; White, A. J. P. *J. Am. Chem. Soc.* **2006**, *128*, 7410−7411.

(26) Allgeier, A. M.; Mirkin, C. A. *Angew. Chem., Int. Ed.* **1998**, *37*, 894−908.

(27) Lorkovic, I. M.; Duff, R. R.; Wrighton, M. S. *J. Am. Chem. Soc.* **1995**, *117*, 3617−3618.

(28) Durkee, D. A.; Eitouni, H. B.; Gomez, E. D.; Ellsworth, M. W.; Bell, A. T.; Balsara, N. R. *Adv. Mater.* **2005**, *17*, 2003−2006.

(29) Glowacki, D. R.; Harvey, J. N.; Mulholland, A. J. *Nat. Chem.* **2012**, *4*, 169−176.

(30) Abou Hamdan, A.; Dementin, S.; Liebgott, P. P.; Gutierrez-Sanz, O.; Richaud, P.; De Lacey, A. L.; Roussett, M.; Bertrand, P.; Cournac, L.; Leger, C. *J. Am. Chem. Soc.* **2012**, *134*, 8368−8371.

(31) Mao, X.; Simeon, F.; Rutledge, G. C.; Hatton, T. A. *Adv. Mater.* **2013**, *25*, 1309−1314.

(32) Mao, X.; Hatton, T. A.; Rutledge, G. C. *Curr. Org. Chem.* **2013**, *17*, 1390−1401.

(33) Mao, X.; Rutledge, G. C.; Hatton, T. A. *Langmuir* **2013**, *29*, 9626−9634.

(34) Akhoury, A.; Bromberg, L.; Hatton, T. A. *ACS Appl. Mater. Interfaces* **2011**, *3*, 1167−1174.

(35) Mao, X.; Simeon, F.; Achilleos, D. S.; Rutledge, G. C.; Hatton, T. A. *J. Mater. Chem. A* **2013**, *1*, 13120−13127.

(36) Jung, M. E. *Comprehensive Organic Synthesis*, Vol. *4*; Pergamon: Oxford, UK, 1991.

(37) Corma, A.; Garcia, H. *Chem. Rev.* **2003**, *103*, 4307−4365.

(38) Sikes, H. D.; Smalley, J. F.; Dudek, S. P.; Cook, A. R.; Newton, M. D.; Chidsey, C. E. D.; Feldberg, S. W. *Science* **2001**, *291*, 1519−1523.

(39) Christoffers, J. *Chem. Commun.* **1997**, 943−944.

(40) Mao, X.; Rutledge, G. C.; Hatton, T. A. *Nano Today* **2014**, *9*, 405−432.

(41) Chen, W.; Fan, Z. L.; Gu, L.; Bao, X. H.; Wang, C. L. *Chem. Commun.* **2010**, *46*, 3905−3907.

DOI: 10.1021/ja512224g
J. Am. Chem. Soc. 2015, 137, 1348−1355